

Generating harmonized SUV within the EANM EARL accreditation program: software approach versus EARL-compliant reconstruction

Charline Lasnon^{1,2,3} · Thibault Salomon¹ · Cédric Desmonts¹ · Pascal Dô⁴ · Youssef Oulkhair⁵ · Jeannick Madelaine⁵ · Nicolas Aide^{1,2,3}

Received: 17 June 2016 / Accepted: 23 October 2016 / Published online: 3 November 2016
© The Japanese Society of Nuclear Medicine 2016

Abstract

Background Evolutions in hardware and software PET technology, such as point spread function (PSF) reconstruction, have been shown to improve diagnostic performance, but can also lead to important device-dependent and reconstruction-dependent variations in standardized uptake values (SUVs). This may preclude the multicentre use of SUVs as a prognostic or diagnostic tool or as a biomarker of the early response to antineoplastic treatments. This study compared two SUV harmonization strategies using a newer reconstruction algorithm that improves lesion detection while maintaining comparability with older systems: (1) the use of a second reconstruction compliant with harmonization standards and (2) the use of a proprietary software tool (EQ.PET). **Methods** PET data from 50 consecutive non-small cell lung cancer patients were reconstructed with PSF reconstruction for optimal tumor detection and an ordered subset

expectation maximization (OSEM3D) reconstruction to mimic a former generation PET. An additional PSF reconstruction was performed with a 7 mm Gaussian filter (PSF₇, first method), and, post-reconstruction, the EQ filter (same Gaussian filter) was applied to the PSF data (PSF_{EQ}, second method) for harmonization purposes. The 7 mm kernel filter was chosen to comply with the European Association of Nuclear Medicine (EANM) standards. SUVs for all reconstructions were compared with regression analyses and/or Bland–Altman plots.

Results Overall, 171 lesions were analyzed: 55 lung lesions (32.2%), 87 lymph nodes (50.9%), and 29 metastases (16.9%). In these lesions, the mean PSF₇/OSEM3D ratios for SUV_{max} and SUV_{peak} were 1.02 (95% CI: 0.93–1.11) and 1.04 (95% CI: 0.95–1.14), respectively. The mean PSF_{EQ}/OSEM3D ratios for SUV_{max} and SUV_{peak} were 1.01 (95% CI: 0.91–1.11) and 1.04 (95% CI: 0.94–1.14), respectively. When comparing PSF₇ and PSF_{EQ}, Bland–Altman analysis showed that the mean PSF₇/PSF_{EQ} ratios for SUV_{max} and SUV_{peak} were 1.01 (95% CI: 0.96–1.06) and 1.01 (95% CI: 0.97–1.04), respectively.

Conclusion The issue of reconstruction dependency in SUV values that hampers the comparison of data between different PET systems can be overcome using two reconstructions for harmonized quantification and optimal diagnosis or using the EQ.PET technology. Both technologies produce similar results, EQ.PET sparing reconstruction and interpretation time. Other manufacturers are encouraged to either emulate this solution or to produce a vendor-neutral approach.

Keywords Positron emission tomography · ¹⁸F-Fluorodeoxyglucose · Quantitation · Standardized uptake value · Harmonization

P. Dô, Y. Oulkhair, and J. Madelaine contributed equally.

Electronic supplementary material The online version of this article (doi:10.1007/s12149-016-1135-2) contains supplementary material, which is available to authorized users.

✉ Nicolas Aide
aide-n@chu-caen.fr

- ¹ Nuclear Medicine Department, Caen University Hospital, Avenue Côte de Nacre, 14000 Caen, France
- ² INSERM 1199, François Baclesse Cancer Centre, Caen, France
- ³ Normandie University, Caen, France
- ⁴ Thoracic Oncology, François Baclesse Cancer Centre, Caen, France
- ⁵ Pulmonology Department, Caen University Hospital, Caen, France

Background

Over the last 20 years, ^{18}F -Fluorodeoxyglucose (^{18}F -FDG) positron emission tomography (PET) has played an increasing role in the management of cancer patients and standardized uptake values (SUVs) have been increasingly used as non-invasive quantitative imaging biomarkers in oncology [1–5]. However, to use SUV as a biomarker in multicentre trials or in sites equipped with multiple PET scanners, adequate reproducibility is required, so that SUVs are comparable regardless of the PET system used.

Hardware and software evolutions can lead to important device-dependent and reconstruction-dependent variations in SUVs. For example, point-spread-function (PSF) reconstruction, which is available from the three major PET vendors and improves spatial resolution throughout the entire field-of-view [6–10], has been shown to significantly improve the diagnostic performance of ^{18}F -FDG PET in various malignancies and to substantially increase SUV values as compared to the former generation OSEM algorithm [11–13]. More recently, Bayesian penalised likelihood (BPL) reconstruction, which can also include PSF modelling, has been reported to increase SUVs and to improve signal-to-noise ratios as compared to the standard PET reconstructions [14–16].

Adequate reproducibility of SUVs can be achieved by harmonizing patient preparation as well as acquisition and reconstruction parameters [17, 18], as recommended by the European Association Research Ltd (EARL) accreditation program [19], the North American Quantitative Imaging Biomarker Alliance (QIBA), and Uniform Protocols in Clinical Trials (UPICT) [20]. With regard to reconstruction-dependent variations, it has been recently shown that it is possible to harmonize SUVs produced by an advanced reconstruction algorithm, to meet harmonizing standards, such as those recommended by the European association of Nuclear Medicine (EANM), by applying a filter during the reconstruction [21]. This method, which is recommended by the EARL accreditation program, requires the reconstruction of two data sets: one for optimal lesion detection and one for harmonized quantification, with NEMA NU-2 phantom-based filtering chosen, so that activity concentration recoveries are as close as possible to those recommended by EANM guidelines. To avoid the reconstruction of two data sets, a proprietary software solution, marketed as EQ.PET (Siemens, Oxford, UK), has been developed to simultaneously allow optimal lesion detection and harmonized quantification from a single data set [22, 23]. This software simultaneously presents the reconstruction that provides optimal lesion detection for diagnostic interpretation with harmonized SUV results (Fig. 1). While the use of a second reconstruction and the EQ.PET technology

have both been validated in large series of tumor lesions [21, 23], they have not yet been confronted to each other to test for inconsistencies. Indeed, as EQ.PET remains a patented automatic software working “behind the scene” without possibility for the imaging specialist to check the adequacy of region of interest placement, there is a need to validate this technology against a gold standard.

Thus, the present study aimed at comparing the two harmonization strategies above-mentioned that enable the use of newer reconstruction algorithms which improve lesion detection while maintaining compatibility of SUV with older systems. As SUV is mainly used for therapy assessment, we mimicked a situation in which a patient would undergo pre- and post-treatment scans on different generation PET systems by reconstructing the same raw PET data with an ordered subset expectation maximization (OSEM) algorithm known to meet EANM requirements and a PSF reconstruction designed for optimal tumor detection. A filter was then applied to the PSF reconstruction to fulfil EANM requirements either by reconstructing a second data set or using the EQ.PET methodology. The OSEM reconstruction and the use of a second data set, which both meet the EANM and EARL requirements, were chosen as standards of reference for SUV quantification and harmonization. We focused on SUV_{max} and SUV_{peak} , the two most frequently used SUV metrics [24, 25]. As SUV reconstruction dependency is not the only source of variability, other technical and biological parameters as well as compliance to EANM guidelines for PET tumor imaging were also analyzed.

Methods

Calibration and cross calibration

The calibration of the PET system was performed daily with a ^{68}Ge cylinder with a known radioactive concentration.

The cross-calibration procedure was performed once during the present study. A solution of ^{18}F -FDG (70.2 MBq, as assessed by the dose calibrator) was introduced into a cylindrical phantom with an exactly known volume and completed with water, which resulted in a solution with an exactly known concentration. A two-bed acquisition of the phantom was performed, and images were reconstructed with attenuation and scatter correction identical to patient studies. Twelve VOIs were drawn on consecutive axial slices to determine the average activity concentration of ^{18}F -FDG within the phantom. The cross-calibration factor was calculated as the ratio of the calculated activity and the true activity. The cross-calibration factor was found to be 1.003.

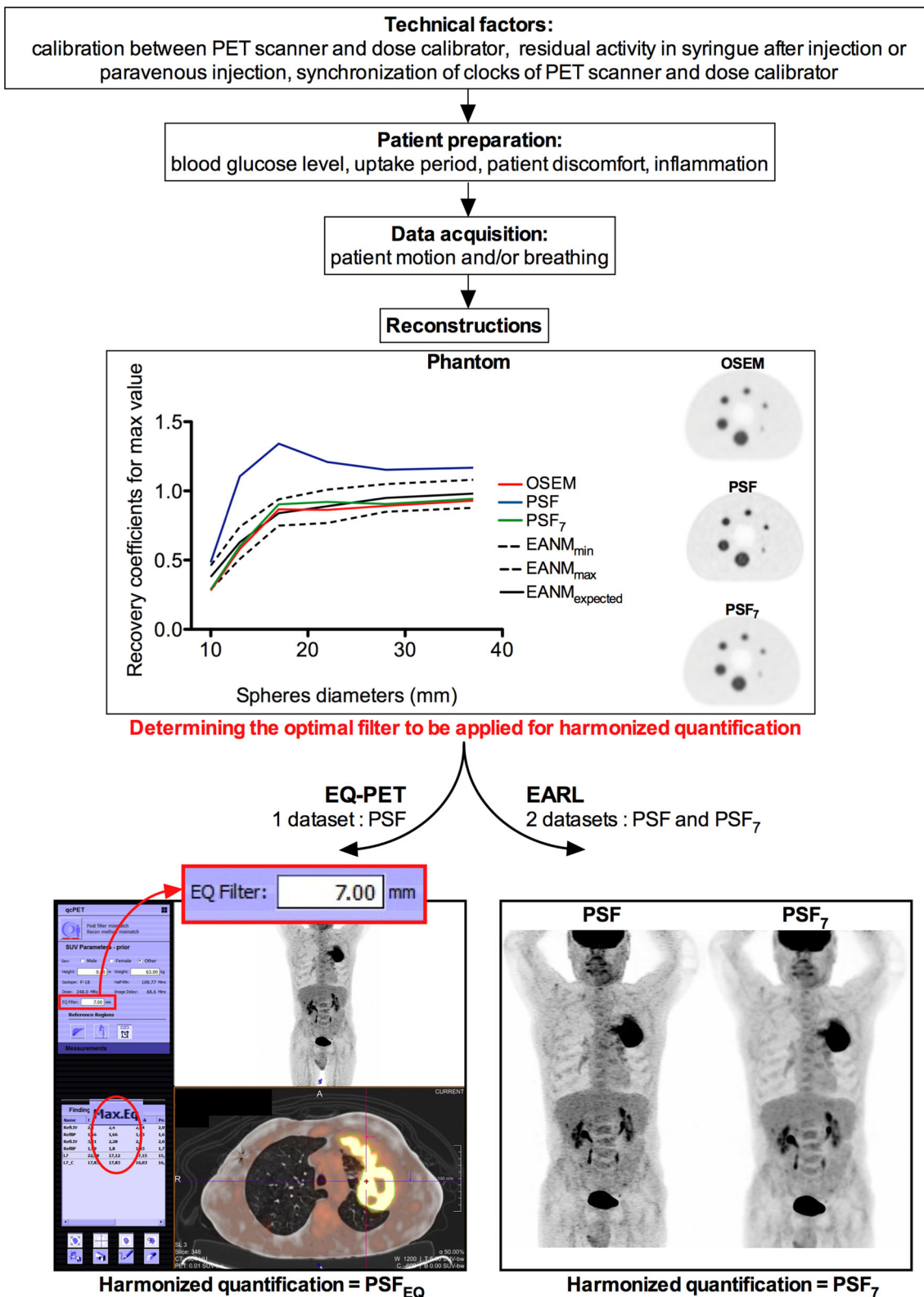


Fig. 1 Illustration of reconstruction harmonization methods and summary of the main factors influencing SUV values

Moreover, clocks of the PET acquisition workstation and that of the dose calibrator were synchronized weekly.

Patient study

This study included 50 consecutive patients referred to our institution for staging and restaging of lung cancer. Informed consent was waived for this type of study by the local ethics committee (Ref A12-D24-VOL13, Comité de protection des personnes Nord-Ouest III), since the scans were performed for clinical indications and the trial procedures were performed independent of usual clinical reporting. The weight and height of patients on the day of the PET examination were recorded. BMI was computed as follows:

$$\text{BMI} = \frac{\text{Weight (kg)}}{\text{Height (m}^2\text{)}}.$$

After a 15-min rest in a warm room, patients who had been fasting for 6 h were injected with 18F-FDG. The injected activity and the exact delay between injection and the start of the acquisition were recorded for each patient.

PET/CT acquisition and reconstruction parameters

All PET imaging studies were performed on a Biograph TrueV (Siemens Medical Solutions) with a 6-slice spiral CT component. Technical details regarding this system can be found elsewhere [6]. CT acquisition was performed first, with the following parameters: 60 mAs, 130 kVp, pitch 1 and 6×2 mm collimation. Subsequently, the PET emission acquisition was performed in 3D mode. Patients were scanned from the skull base to the mid-thighs.

In our department, PET images are reconstructed with a PSF reconstruction algorithm (HD; TrueX, Siemens Medical Solutions; 3 iterations and 21 subsets) without filtering. For the purpose of this study, raw data were also reconstructed with the OSEM3D reconstruction algorithm (4 iterations and 8 subsets) and a PSF reconstruction algorithm (HD; TrueX, Siemens Medical Solutions; 3 iterations and 21 subsets) using a 7 mm Gaussian filter (PSF₇). As shown in a previous study, this latter reconstruction led to protocol-specific images with NEMA NU-2 phantom-based filtering that meet EANM quantitative harmonizing standards, therefore, reducing reconstruction-dependent variation in SUVs [21]. The OSEM3D reconstruction parameters were chosen as recommended by the manufacturer. These parameters meet the EANM requirements regarding activity recoveries.

For all reconstructions, matrix size was 168×168 , resulting in a $4.07 \times 4.07 \times 4.07$ mm voxel size. Scatter and attenuation corrections were applied.

Only the PSF-reconstructed data without filtering were used for the purpose of diagnostic workup.

PET/CT analysis

The same reader analyzed all PET data on a prototype implementation of the EQ.PET functionality that is available for clinical use in Syngo.via (Siemens Medical Solutions).

The first reconstructions displayed on the screen were the PSF and the OSEM3D reconstructions. The EQ.PET filtered SUVs were calculated behind the scenes, without showing the filtered image. The EQ.PET filter for PSF reconstruction was set to 7 mm to meet the kernel of 7 mm of the PSF₇ reconstruction. On the PSF reconstruction, VOIs with a 50% isocontour were drawn on primary tumor lesions, and mediastinal and hilar nodes considered to have pathologically increased uptake and metastatic lesions. The slice number from which has been drawn the volume of interest was noted. The VOIs were then automatically propagated on the OSEM3D reconstruction by re-computing a 50% isocontour at the same location as in the PSF data set. This allowed computing SUV_{max} and SUV_{peak} for PSF, OSEM3D, and PSF_{EQ}.

The second sets of reconstructions displayed on the screen were PSF and PSF₇ reconstructions. Previous VOIs with a 50% isocontour were redrawn identically on PSF reconstruction using slice numbers previously noted. The VOIs were then automatically propagated on the PSF₇ reconstruction by re-computing a 50% isocontour at the same location as in the PSF data set. This allowed computing SUV_{max} and SUV_{peak} PSF₇ on the same location than previously did for the PSF and OSEM3D reconstructions.

SUV_{peak} was defined as a 1-cm³ sphere positioned within the lesion so as to maximise the enclosed average SUV. Background activity was measured as SUV_{peak} and SUV_{mean} in an automatically placed 3 cm diameter sphere in the right liver lobe.

For all lesions, SUV_{max} and SUV_{peak} were recorded for PSF, PSF_{EQ}, OSEM3D, and PSF₇. For this study, SUV_{peak} was not corrected for lean body mass.

Finally, short-axis dimension (mm), as determined on axial CT slices, was recorded for lesion when applicable.

Statistical analysis

Quantitative data from clinical PET/CT examinations are presented as mean (standard deviation, SD) and median when appropriate. The relationship between PSF, PSF_{EQ}, OSEM, and PSF₇ quantitative values was assessed with Bland–Altman plots. Ratios between PSF_{EQ} and PSF₇ quantitative values (for SUV_{max}, and SUV_{peak}) according

to patient's BMI and location and size of the lesions were compared using the Kruskal–Wallis test for multiple group comparison or the Mann–Whitney test when appropriate. For lesion size, the ratios between PSF_{EQ} and PSF₇ SUVs were dichotomized in 3 groups (<10, 10–20, and >20 mm). For all tests, a two-tailed P value of less than 0.05 was considered statistically significant. Graphs and analyses were carried out using the GraphPad software.

Availability of data and materials

The data sets supporting the conclusions of this article are available upon request.

Results

Population characteristics and compliance to guidelines for tumor imaging

Clinical data are summarized in Table 1. The mean (SD) administered ¹⁸F-FDG dose was 4.00 (0.16) MBq/kg. The mean (SD) delay between the administration of ¹⁸F-FDG and the start of the PET acquisition was 60 (3.24) min. Overall, the EANM 2.0 guidelines for PET tumor imaging were fulfilled in 48/50 patients (96%). At the time of injection, the mean (SD) blood glucose level was 5.70 (1.27) mmol/l.

Validation of the EQ-PET technology and the use of an additional harmonized PET data set to overcome reconstruction dependency of SUVs

Overall, 171 VOIs were drawn over 55 lung lesions (32.2%), 87 lymph nodes (50.9%), and 29 metastases

Table 1 Patient demographics

Characteristic	
Sex ratio (M/F)	3.5
Age (years)	
Range	37–90
Mean (SD)	65 (10.99)
Body habitus, <i>n</i> (%)	
BMI ≤25	32 (64)
BMI >25	18 (36)
Histological diagnosis, <i>n</i> (%)	
Small cell lung cancer	4 (8)
Non small cell lung cancer	46 (92)
Squamous cell carcinoma	24 (52.2)
Adenocarcinoma	16 (34.8)
Large cell lung cancer	6 (13.0)

(16.9%). All lesions confounded, the mean SUV_{max} (SD) was 10.93 (7.03), 6.96 (4.36), 7.05 (4.36), and 7.01 (4.36) for PSF, OSEM3D, PSF₇ reconstructions, and PSF_{EQ}, respectively. The mean SUV_{peak} (SD) was 6.82 (4.29), 5.41 (3.59), 5.60 (3.59), and 5.58 (3.59) for PSF, OSEM3D, PSF₇ reconstructions, and PSF_{EQ}, respectively.

As shown in Fig. 2, the mean ratios between PSF and OSEM3D reconstructions for SUV_{max} and SUV_{peak} were 1.59 (95% CI: 1.12–2.06) and 1.28 (95% CI: 1.08–1.49), respectively. When using the filtered PSF₇ reconstruction, the mean ratios between PSF₇ and OSEM3D for SUV_{max} and SUV_{peak} were 1.02 (95% CI: 0.93–1.11) and 1.04 (95% CI: 0.95–1.14), respectively. After application of the EQ.PET filter, the mean ratios between PSF_{EQ} and OSEM3D for SUV_{max} and SUV_{peak} were 1.01 (95% CI: 0.91–1.11) and 1.04 (95% CI: 0.94–1.14), respectively.

When comparing PSF₇ and PSF_{EQ} standardized uptake values, a perfect correlation was found with an *r*² to 1.00 for both SUV_{max} and SUV_{peak} values (*p* < 0.0001). Regarding Bland–Altman analysis, the mean ratios were 1.01 (95% CI: 0.96–1.06) and 1.01 (95% CI: 0.97–1.04) for SUV_{max} and SUV_{peak}, respectively (Fig. 3a).

Outliers of all Bland–Altman plots are summarized in Table 2, and 75% of them corresponded to lymph nodes lesion with a median size equals 9.76 mm. Median size of outlier tumors was 19.39 mm.

Effect of harmonization strategies on the liver background

The mean SUV_{mean} (SD) was 2.36 (0.37), 2.39 (0.37), 2.36 (0.37), and 2.36 (0.37) for PSF, OSEM3D, PSF₇ reconstructions, and PSF_{EQ}, respectively. The mean SUV_{peak} (SD) was 2.90 (0.46), 2.72 (0.43), 2.74 (0.44), and 2.73 (0.44) for PSF, OSEM3D, PSF₇ reconstructions, and PSF_{EQ}, respectively.

Bland–Altman plots are displayed in supplemental Fig. 1. The mean ratios between PSF and OSEM3D reconstructions for SUV_{mean} and SUV_{peak} were 0.99 (95% CI = 0.96–1.02) and 1.06 (95% CI: 1.02–1.11), respectively. When using filtered PSF₇ reconstruction, the mean ratios between PSF₇ and OSEM3D for SUV_{mean} and SUV_{peak} were 0.99 (95% CI: 0.97–1.01) and 1.00 (95% CI: 0.97–1.03), respectively. After application of the EQ.PET filter, the mean ratios between PSF_{EQ} and OSEM3D for SUV_{mean} and SUV_{peak} were 1.01 (95% CI: 0.99–1.04) and 1.00 (95% CI: 0.97–1.04), respectively.

When comparing PSF₇ and PSF_{EQ}, a perfect correlation was found with an *r*² to 1.00 for both SUV_{mean} and SUV_{peak} values (*p* < 0.0001). Regarding Bland–Altman analysis, the mean ratios were 1.00 (95% CI: 1.00–1.00) and 1.00 (95% CI: 0.99–1.01) for SUV_{mean} and SUV_{peak}, respectively (Fig. 3b).

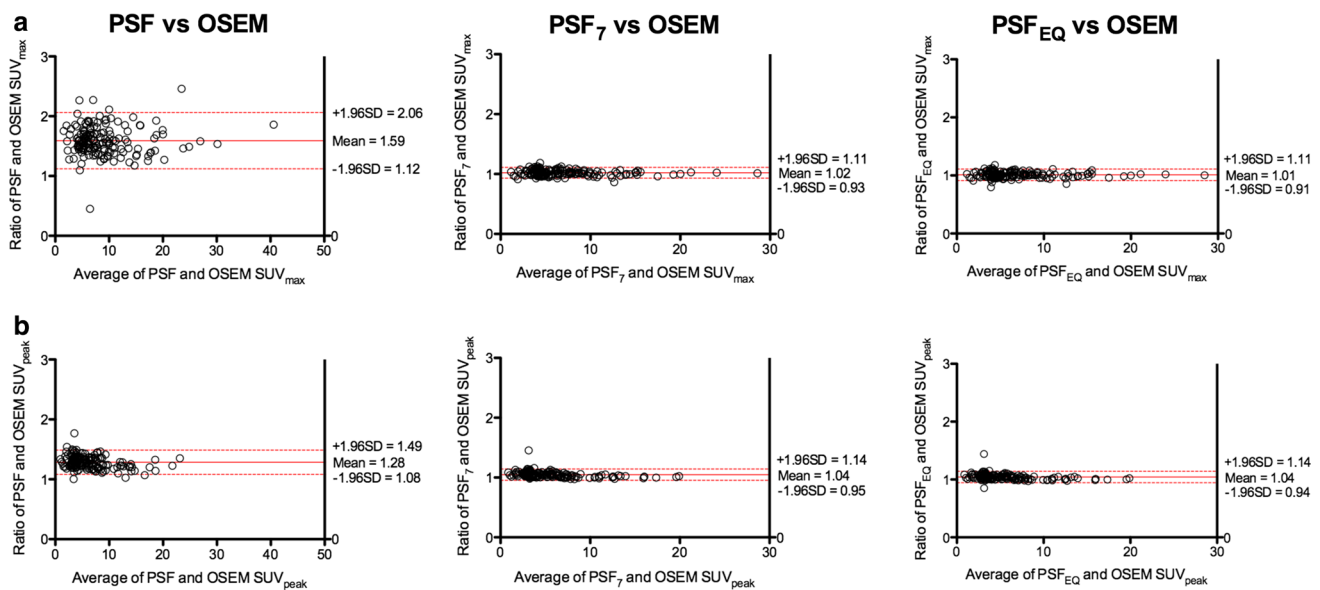


Fig. 2 Validation of the EQ-PET technology and the use of an additional harmonized PET data set to overcome reconstruction dependency of SUVs. For *left to right*, PSF and OSEM3D values,

PSF₇ and OSEM3D values, and PSF_{EQ} and OSEM3D values were compared using Bland–Altman plots. *Upper panel (a)* displays SUV_{max} values, and *lower panel (b)* displays SUV_{peak} values

Confounding factors

For 16 lesions, the measurement of the short dimension was not applicable: 3 primary lung lesions, 2 pleural metastases, 10 bone metastases, and 1 pulmonary metastasis with either no visible lesion or blurring contours on computed tomography.

As shown in Fig. 4, the ratios between PSF₇ and PSF_{EQ} quantitative values (SUV_{max} and SUV_{peak}) were not different according to the histological type of the primary lesion, the patient BMI, or the location of lesion. When considering the size of the lesion, ratios between PSF₇ and PSF_{EQ} quantitative values (SUV_{max} and SUV_{peak}) were significantly different between <10 and >20 mm groups. Mean ratios and their standard deviations tended to be higher for the smallest lesions, but all ratios were found to be within the 1.05 limit.

Discussion

Accurate and reproducible SUVs are mandatory when using these metrics as quantitative imaging biomarkers in multicentre studies. This can be achieved by harmonizing both patient preparation as well as acquisition and reconstruction parameters [17, 18], as recommended by the European Association Research Ltd (EARL) accreditation program [19], and other groups [20]. Harmonization of the reconstructions parameters may be challenging, because centres running PET systems with new reconstruction algorithms participating in multicentre trials often wish to

use their PET system with parameters chosen to achieve optimal lesion detection. In addition, centres using similar PET systems may use different reconstructions or filtering parameters [26], highlighting the need to harmonize quantitative values even within centres running a similar equipment.

The present study compared two solutions to harmonize SUV to a given standard; here, the EANM harmonizing standards: (1) the use of two data sets: one for optimal lesion detection and one for harmonized quantification [21] and (2) the use of a proprietary software that has been developed to simultaneously allow optimal lesion detection and harmonized quantification from a single data set [23].

As reconstruction is not the only source of variability in SUV measurements, we analyzed adherence to EANM guidelines for PET tumor imaging, especially with regard to other technical factors susceptible to hamper accuracy and reproducibility of SUVs. Compliance was found to be good for clocks synchronization, cross calibrations between the PET system and the dose calibrator, standardized injected dose, and uptake time. Despite this good compliance, when mimicking the situation in which a patient would undergo pre- and post-treatment scans on different generation PET systems by reconstructing the same raw PET data with an OSEM algorithm known to meet EANM requirements and a PSF reconstruction designed for optimal tumor detection, a substantial increase in SUV_{max} and SUV_{peak} was noticed for PSF images. Mean ratios between OSEM3D and PSF images were 1.59 for SUV_{max} and 1.28 for SUV_{peak}. Taking the example of a system upgrade during a trial, this 59% increase in PSF-

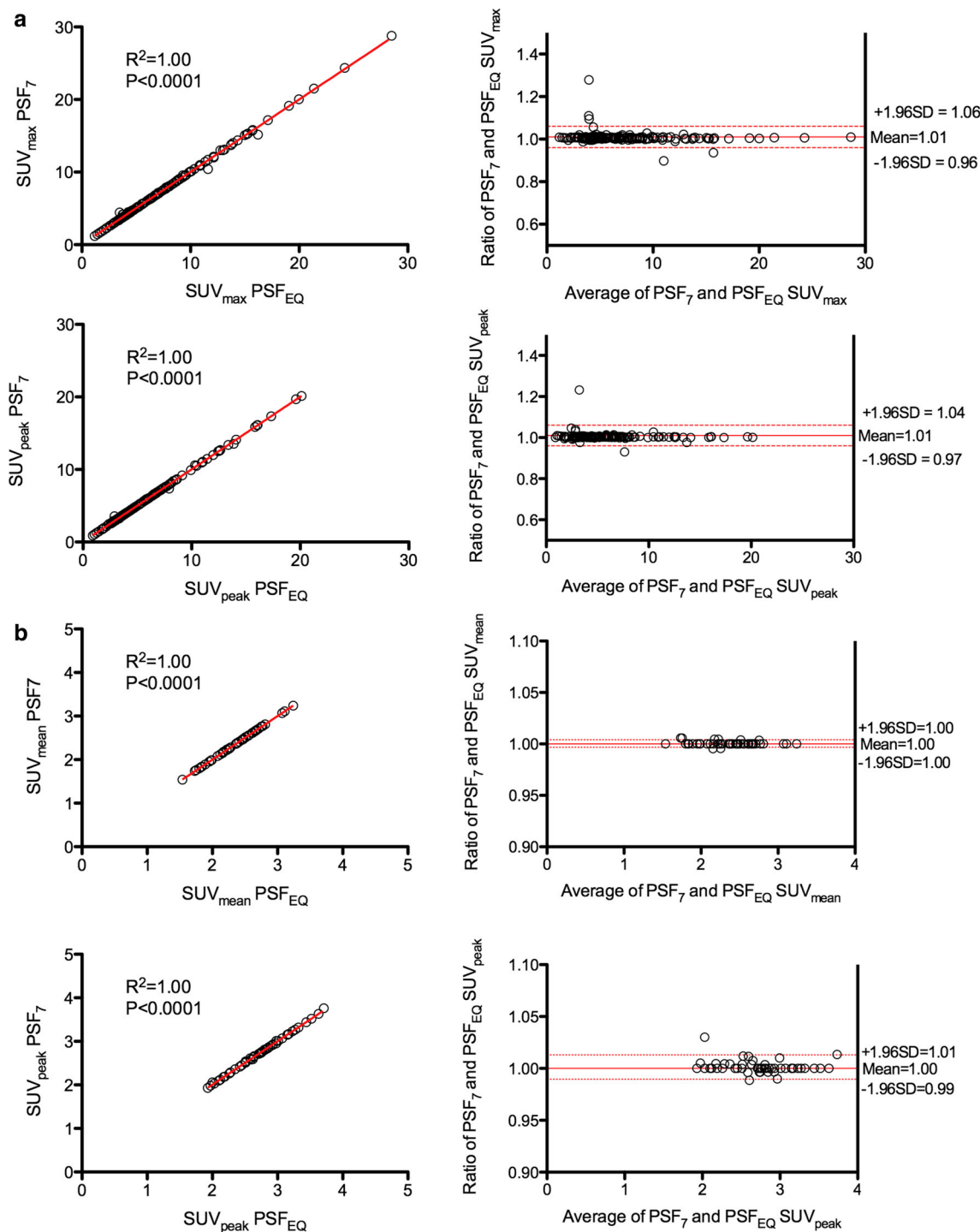


Fig. 3 Pairwise comparison of the EQ-PET technology and the use of an additional harmonized PET data set. The *upper panel* (a) displays linear regression and Bland–Altman analysis for

SUV_{max} and SUV_{peak} values of tumoral lesions. The *lower panel* (b) displays linear regression and Bland–Altman analysis for SUV_{mean} and SUV_{peak} values of liver background

reconstructed images would be likely to impact therapy assessment either with the EORTC and the PERCIST criteria for which a 25 and 30% increase in SUV define progressive disease, respectively [27]. We found that after having applied an appropriate filter (in this study, a 7 mm

Gaussian filter), the mean ratios between OSEM and PSF₇ data for SUV_{max} and SUV_{peak} were 1.02 and 1.04, respectively, with very narrow confidence intervals. Similar results were found after the use of the EQ-PET technology. Thus, our study supports previous studies

Table 2 Details of Bland–Altman plot outliers

	SUV _{max} (n)		SUV _{peak} (n)	
	Above the upper limit of confidence	Below the lower limit of confidence	Above the upper limit of confidence	Below the lower limit of confidence
Ratio of PSF ₇ and OSEM3D	5 (2LN, 2T, 1 M)	5 (4 LN, 1T)	3 (2LN, 1T)	0
Ratio of PSF _{EQ} and OSEM3D	5 (3LN, 2T)	4 (4LN)	2 (2LN)	1 (1LN)
Ratio of PSF ₇ and PSF _{EQ}	3 (3LN)	2 (1LN, 1T)	2 (2LN)	1 (1LN)

LN lymph node, T primary lung tumor, M metastasis

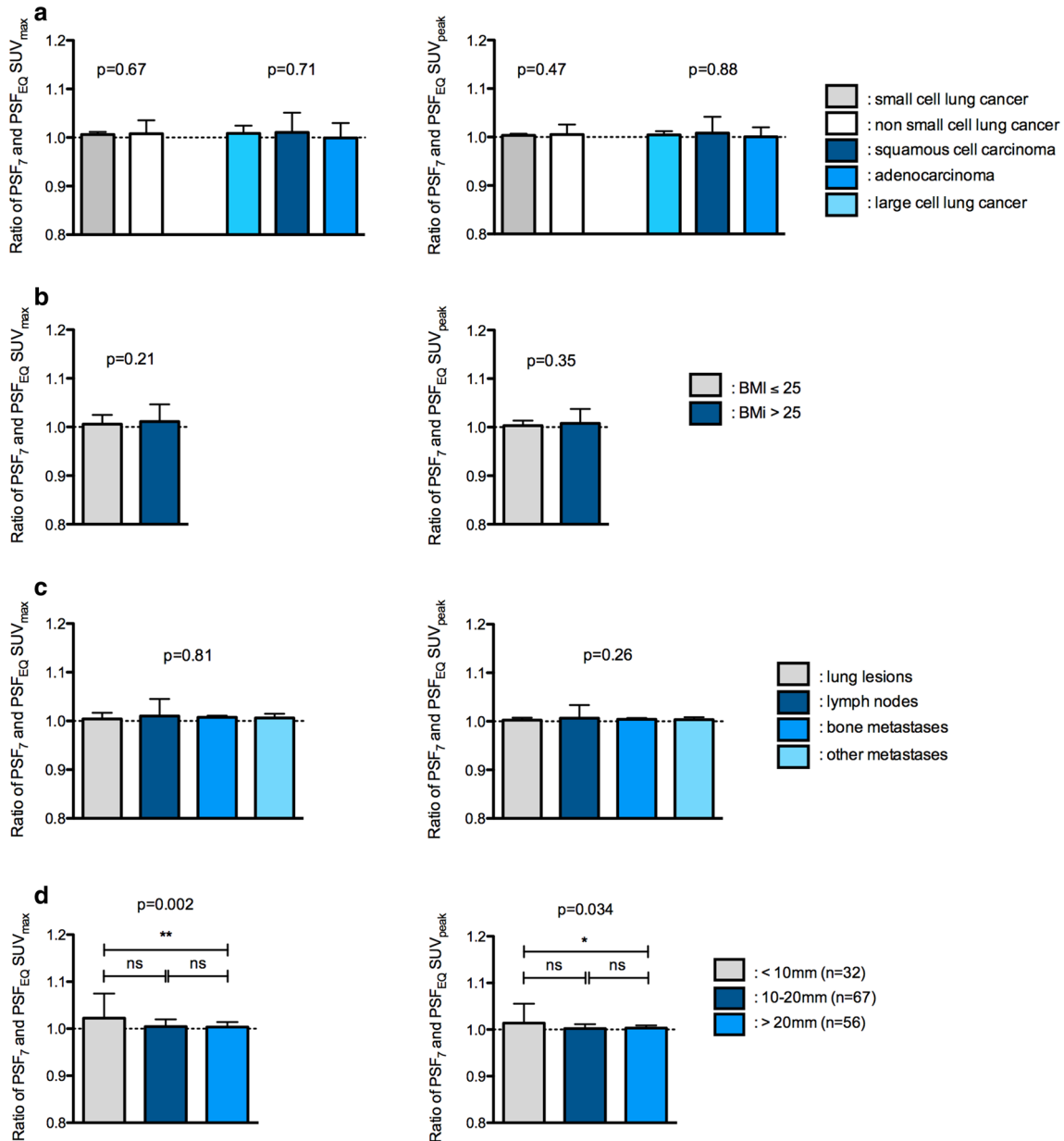


Fig. 4 Impact of confounding factors. Impact of the histology of the primary lung lesion (a), the BMI (b), the location of the lesion (c), and the lesion size (d) on the ratio between PSF₇ and PSF_{EQ}

quantitative values (left panels SUV_{max} and right panels SUV_{peak}). Note that 16 lesions were not measurable and are, therefore, not included in the “per size” analysis (d)

concluding that both methods are appropriate to harmonize data and show that they give almost similar results either for SUV_{max} or SUV_{peak} values. Regarding Bland–Altman analysis comparing PSF_7 and PSF_{EQ} , there were few outliers, which occurred mainly for lymph node lesions and/or smallest lesions. Of note, there were fewer outliers when using SUV_{peak} values. Histological type of primary lung cancer, and patient's BMI and localisation of the lesion were not found to be confounding factors. When considering the size of the lesion, ratios between PSF_7 and PSF_{EQ} quantitative values were significantly different between <10 and >20 mm groups both for SUV_{max} and SUV_{peak} values, thus suggesting that it exists a difference between the two harmonization strategies based on the size of the lesion. These results could be explained by the fact that the size of the lesion was found to be a confounding factor for PSF_{EQ} , whereas it was not for PSF_7 [12, 23]. One can notice that the standard deviations were higher for the smallest lesions suggesting that differences between the two methods of harmonization were mainly present for the smallest lesions and are likely to be due to partial volume effect. However, the differences observed between groups in our study were extremely small with PSF_7/PSF_{EQ} ratios ranging only from 1.002 to 1.022 and so had certainly no clinical significance.

Considering liver background, it is supposed to have less reconstruction dependency than tumoral uptake. This is the reason why it has been recommended to proceed to a normalization of tumoral uptake by liver background [28] and why liver background is used as a reference in the Deauville Scale (DS) when assessing therapy response in lymphoma. Our results showed no influence of PSF reconstruction on liver uptake, as the mean ratio between PSF and OSEM reconstruction was equal to 0.99 with narrow confidence interval. Therefore, the tumor/liver ratio could not be used to overcome reconstruction dependency. This finding is important in the context of ongoing efforts to further improve the DS using a semi-quantitative extension [29, 30]. In that setting, harmonization of SUVs from pooled PET data would produce optimal lesion/liver ratios and discrimination between DS 4 and DS 5.

Our study showed that using two reconstructions for harmonized quantification and optimal diagnosis and the EQ.PET technology equally overcame reconstruction dependency in SUVs values. The choice, therefore, remains open to use one or the other of these methods. However, a potential issue is that the EQ software will certainly be used by departments using Siemens medical solution equipment, whereas the use of a second reconstruction data set, recommended by the EARL accreditation program for quantitation, can be easily implemented in any PET unit. This is actually the main limitation of our work: we used a Siemens software only on a Siemens PET system, thereby limiting the exportation of

these results to departments equipped by the same vendor. Indeed, the ability of EQ technology to process images acquired on non-Siemens PET systems has not been addressed here and would require validation of the software's vendor-neutral capacity, using clinical data and other tools, such as the digital reference object technique recently published by Pierce and co-workers [31]. Nonetheless, the EQ.PET software is the quickest method, as it does not require a second standardized reconstruction that has to be stored. The EQ.PET software could then be applied to older examinations, acquired and stored before the era of PET standardization, and provided that other sources of SUV variability are controlled and data regarding calibration of the PET system is available. Finally, for this study, the current EANM expected values were set as the reference standard, but the EQ.PET filter could be adapted to meet any given standard. This is important in the context of evolving guidelines.

Conclusion

The reconstruction dependency in SUV metrics impedes comparison of quantitative data between different PET systems and requires harmonizing SUVs. Harmonization can be achieved using a second reconstruction for harmonized quantification in addition to the reconstruction optimised for diagnostic purpose or using a software solution that allows optimal lesion detection and harmonized quantification from a single data set. Both technologies produced similar results, but the software solution has the advantages of saving reconstruction and interpretation time and allowing for retrospective analysis of stored data.

Acknowledgements Dr. Alison Johnson, François Baclesse cancer Centre, France, is thanked for her critical review of the manuscript.

Compliance with ethical standards

Conflict of interest disclosure None.

Ethics approval Informed consent was waived for this type of study by the local ethics committee (*Ref A12-D24-VOL13, Comité de protection des personnes Nord-Ouest III*).

References

1. Bengtsson T, Hicks RJ, Peterson A, Port RE. 18F-FDG PET as a surrogate biomarker in non-small cell lung cancer treated with erlotinib: newly identified lesions are more informative than standardized uptake value. *J Nucl Med*. 2012;53:530–7. doi:10.2967/jnumed.111.092544.
2. Konings R, van Gool MH, Bard MP, Zwijnenburg A, Titulaer BM, Aukema TS, et al. Prognostic value of pre-operative glucose-corrected maximum standardized uptake value in patients with non-small cell lung cancer after complete surgical resection

- and 5-year follow-up. *Ann Nucl Med.* 2016;30:362–8. doi:[10.1007/s12149-016-1070-2](https://doi.org/10.1007/s12149-016-1070-2).
3. Kremer R, Peysakhovich Y, Dan LF, Guralnik L, Kagna O, Nir RR, et al. FDG PET/CT for assessing the resectability of NSCLC patients with N2 disease after neoadjuvant therapy. *Ann Nucl Med.* 2016;30:114–21. doi:[10.1007/s12149-015-1038-7](https://doi.org/10.1007/s12149-015-1038-7).
 4. Shigemoto Y, Suga K, Matsunaga N. F-18-FDG-avid lymph node metastasis along preferential lymphatic drainage pathways from the tumor-bearing lung lobe on F-18-FDG PET/CT in patients with non-small-cell lung cancer. *Ann Nucl Med.* 2016;30:287–97. doi:[10.1007/s12149-016-1063-1](https://doi.org/10.1007/s12149-016-1063-1).
 5. Yamamoto T, Kadoya N, Shirata Y, Kaneta T, Koto M, Umezawa R, et al. Formula corrected maximal standardized uptake value in FDG-PET for partial volume effect and motion artifact is not a prognostic factor in stage I non-small cell lung cancer treated with stereotactic body radiotherapy. *Ann Nucl Med.* 2015;29:666–73. doi:[10.1007/s12149-015-0991-5](https://doi.org/10.1007/s12149-015-0991-5).
 6. Lee YS, Kim JS, Kim KM, Kang JH, Lim SM, Kim HJ. Performance measurement of PSF modeling reconstruction (True X) on Siemens Biograph TruePoint TrueV PET/CT. *Ann Nucl Med.* 2014;28:340–8. doi:[10.1007/s12149-014-0815-z](https://doi.org/10.1007/s12149-014-0815-z).
 7. Panin VY, Kehren F, Michel C, Casey M. Fully 3-D PET reconstruction with system matrix derived from point source measurements. *IEEE Trans Med Imaging.* 2006;25:907–21.
 8. Taniguchi T, Akamatsu G, Kasahara Y, Mitsumoto K, Baba S, Tsutsui Y, et al. Improvement in PET/CT image quality in overweight patients with PSF and TOF. *Ann Nucl Med.* 2015;29:71–7. doi:[10.1007/s12149-014-0912-z](https://doi.org/10.1007/s12149-014-0912-z).
 9. Tong S, Alessio AM, Kinahan PE. Evaluation of noise properties in PSF-based PET image reconstruction. *IEEE Nucl Sci Symp Conf Rec.* 1997;2009(2009):3042–7.
 10. Tong S, Alessio AM, Kinahan PE. Noise and signal properties in PSF-based fully 3D PET image reconstruction: an experimental evaluation. *Phys Med Biol.* 2010;55:1453–73. doi:[10.1088/0031-9155/55/5/013](https://doi.org/10.1088/0031-9155/55/5/013).
 11. Bellevre D, Blanc Fournier C, Switers O, Dugue AE, Levy C, Allouache D, et al. Staging the axilla in breast cancer patients with (1)(8)F-FDG PET: how small are the metastases that we can detect with new generation clinical PET systems? *Eur J Nucl Med Mol Imaging.* 2014;41:1103–12. doi:[10.1007/s00259-014-2689-7](https://doi.org/10.1007/s00259-014-2689-7).
 12. Lasnon C, Hicks RJ, Beaugard JM, Milner A, Paciencia M, Guizard AV, et al. Impact of point spread function reconstruction on thoracic lymph node staging with 18F-FDG PET/CT in non-small cell lung cancer. *Clin Nucl Med.* 2012;37:971–6. doi:[10.1097/RLU.0b013e318251e3d1](https://doi.org/10.1097/RLU.0b013e318251e3d1).
 13. Rogasch JM, Steffen IG, Hofheinz F, Grosser OS, Furth C, Mohnike K, et al. The association of tumor-to-background ratios and SUVmax deviations related to point spread function and time-of-flight F18-FDG-PET/CT reconstruction in colorectal liver metastases. *EJNMMI Res.* 2015;5:31. doi:[10.1186/s13550-015-0111-5](https://doi.org/10.1186/s13550-015-0111-5).
 14. Parvizi N, Franklin JM, McGowan DR, Teoh EJ, Bradley KM, Gleeson FV. Does a novel penalized likelihood reconstruction of 18F-FDG PET-CT improve signal-to-background in colorectal liver metastases? *Eur J Radiol.* 2015;. doi:[10.1016/j.ejrad.2015.06.025](https://doi.org/10.1016/j.ejrad.2015.06.025).
 15. Teoh EJ, McGowan DR, Bradley KM, Belcher E, Black E, Gleeson FV. Novel penalised likelihood reconstruction of PET in the assessment of histologically verified small pulmonary nodules. *Eur Radiol.* 2015;. doi:[10.1007/s00330-015-3832-y](https://doi.org/10.1007/s00330-015-3832-y).
 16. Teoh EJ, McGowan DR, Macpherson RE, Bradley KM, Gleeson FV. Phantom and clinical evaluation of the Bayesian penalized likelihood reconstruction algorithm Q.Clear on an LYSO PET/CT system. *J Nucl Med.* 2015;. doi:[10.2967/jnumed.115.159301](https://doi.org/10.2967/jnumed.115.159301).
 17. Boellaard R, Delgado-Bolton R, Oyen WJ, Giammarile F, Tatsch K, Eschner W, et al. FDG PET/CT: EANM procedure guidelines for tumour imaging: version 2.0. *Eur J Nucl Med Mol Imaging.* 2015;42:328–54. doi:[10.1007/s00259-014-2961-x](https://doi.org/10.1007/s00259-014-2961-x).
 18. Boellaard R, O'Doherty MJ, Weber WA, Mottaghy FM, Lonsdale MN, Stroobants SG, et al. FDG PET and PET/CT: EANM procedure guidelines for tumour PET imaging: version 1.0. *Eur J Nucl Med Mol Imaging.* 2010;37:181–200. doi:[10.1007/s00259-009-1297-4](https://doi.org/10.1007/s00259-009-1297-4).
 19. da Silva AM, Fischer A. WE-AB-204-05: harmonizing PET/CT quantification in multicenter studies: a case study. *Med Phys.* 2015;42:3660. doi:[10.1118/1.4925881](https://doi.org/10.1118/1.4925881).
 20. Graham MM, Wahl RL, Hoffman JM, Yap JT, Sunderland JJ, Boellaard R, et al. Summary of the UPICT protocol for 18F-FDG PET/CT imaging in oncology clinical trials. *J Nucl Med.* 2015;56:955–61. doi:[10.2967/jnumed.115.158402](https://doi.org/10.2967/jnumed.115.158402).
 21. Lasnon C, Desmots C, Quak E, Gervais R, Do P, Dubos-Arvis C, et al. Harmonizing SUVs in multicentre trials when using different generation PET systems: prospective validation in non-small cell lung cancer patients. *Eur J Nucl Med Mol Imaging.* 2013;40:985–96. doi:[10.1007/s00259-013-2391-1](https://doi.org/10.1007/s00259-013-2391-1).
 22. Kelly MD, Declerck JM. SUVref: reducing reconstruction-dependent variation in PET SUV. *EJNMMI Res.* 2011;1:16. doi:[10.1186/2191-219X-1-16](https://doi.org/10.1186/2191-219X-1-16).
 23. Quak E, Le Roux PY, Hofman MS, Robin P, Bourhis D, Callahan J, et al. Harmonizing FDG PET quantification while maintaining optimal lesion detection: prospective multicentre validation in 517 oncology patients. *Eur J Nucl Med Mol Imaging.* 2015;42:2072. doi:[10.1007/s00259-015-3128-0](https://doi.org/10.1007/s00259-015-3128-0).
 24. Laffon E, Lamare F, de Clermont H, Burger IA, Marthan R. Variability of average SUV from several hottest voxels is lower than that of SUVmax and SUVpeak. *Eur Radiol.* 2014;24:1964–70. doi:[10.1007/s00330-014-3222-x](https://doi.org/10.1007/s00330-014-3222-x).
 25. Lodge MA, Chaudhry MA, Wahl RL. Noise considerations for PET quantification using maximum and peak standardized uptake value. *J Nucl Med.* 2012;53:1041–7. doi:[10.2967/jnumed.111.101733](https://doi.org/10.2967/jnumed.111.101733).
 26. Sunderland JJ, Christian PE. Quantitative PET/CT scanner performance characterization based upon the society of nuclear medicine and molecular imaging clinical trials network oncology clinical simulator phantom. *J Nucl Med.* 2015;56:145–52. doi:[10.2967/jnumed.114.148056](https://doi.org/10.2967/jnumed.114.148056).
 27. Quak E, Le Roux PY, Lasnon C, Robin P, Hofman MS, Bourhis D, et al. Does PET SUV harmonization affect PERCIST response classification? *J Nucl Med.* 2016. doi:[10.2967/jnumed.115.171983](https://doi.org/10.2967/jnumed.115.171983).
 28. Kuhnert G, Boellaard R, Sterzer S, Kahraman D, Scheffler M, Wolf J, et al. Impact of PET/CT image reconstruction methods and liver uptake normalization strategies on quantitative image analysis. *Eur J Nucl Med Mol Imaging.* 2015;. doi:[10.1007/s00259-015-3165-8](https://doi.org/10.1007/s00259-015-3165-8).
 29. Hasenclever D, Kurch L, Kluge R. Sources of variability in FDG PET imaging and the qPET value: reply to Laffon and Marthan. *Eur J Nucl Med Mol Imaging.* 2014;41:2155–7. doi:[10.1007/s00259-014-2880-x](https://doi.org/10.1007/s00259-014-2880-x).
 30. Hasenclever D, Kurch L, Mauz-Korholz C, Elsner A, Georgi T, Wallace H, et al. qPET - a quantitative extension of the Deauville scale to assess response in interim FDG-PET scans in lymphoma. *Eur J Nucl Med Mol Imaging.* 2014;41:1301–8. doi:[10.1007/s00259-014-2715-9](https://doi.org/10.1007/s00259-014-2715-9).
 31. Pierce LA 2nd, Elston BF, Clunie DA, Nelson D, Kinahan PE. A digital reference object to analyze calculation accuracy of PET standardized uptake value. *Radiology.* 2015;277:538–45. doi:[10.1148/radiol.2015141262](https://doi.org/10.1148/radiol.2015141262).